Exact conditions for ensemble density functional theory

Thais R. Scott [1], John Kozlowski [1], Steven Crisostomo [2], Aurora Pribram-Jones [3], and Kieron Burke [1,2]

[1]*Department of Chemistry, University of California, Irvine, California 92697, USA*
[2]*Department of Physics & Astronomy, University of California, Irvine, California 92697, USA*
[3]*Department of Chemistry, University of California, Merced, California 95343, USA*

Ensemble density functional theory (EDFT) is a promising alternative to time-dependent density functional theory for computing electronic excitation energies. Using coordinate scaling, we prove several fundamental exact conditions in EDFT and illustrate them on the exact singlet bi-ensemble of the Hubbard dimer. Several approximations violate these conditions, and some ground-state conditions from quantum chemistry do not generalize to EDFT. The strong correlation limit is derived for the dimer, revealing weight-dependent derivative discontinuities in EDFT.

I. INTRODUCTION

Sophisticated functional approximations and a relatively low computational cost have made density functional theory [1,2] (DFT) the prevailing method used in electronic structure calculations [3–7]. Currently, the most popular way to access excited states in the DFT formalism is through time-dependent DFT (TDDFT) [7–11], which has been used to predict electronic excitation spectra among other properties. Although TDDFT has been incredibly successful [11], standard approximations fail to replicate charge-transfer excitation energies [12], correctly locate conical intersections [13], or recover double excitations [11] without an *ad hoc* dressing [14]. A less well-known but comparably rigorous alternative to TDDFT is ensemble density functional theory [15–17] (EDFT), which is currently experiencing a renaissance [18–35]. As the EDFT field is revived, it is important to find exact conditions that can be enforced on newly developed EDFT approximations. This is especially important in EDFT, where the choice of ensemble weights is unlimited (assuming they are normalized and are monotonically nonincreasing with energy) and can significantly impact the accuracy of the energies.

Exact conditions were essential for developing accurate approximate functionals in ground-state DFT, and we expect them to be even more critical in EDFT [36–38]. Recently, it was shown that, for realistic Coulombic densities, many popular approximate functionals satisfy or partially satisfy many exact conditions [38]. Thus, a crucial question is which, if any, such conditions can be generalized to ensemble density functional theory?

Motivated by the complexity of the ensemble framework, there have been significant developments towards understanding the limits of the exact ensemble energy. Two examples are the work by Gould [39], which is based on scaling to the strongly correlated regime, and the thorough analysis of the exact energies in the work of Nagy [40]. These works and others are based on fundamental scaling relationships that should apply to both ground states and an ensemble framework but are not explicitly derived and validated. Many of these conditions were initially proven for the ground state by Perdew and Levy [37]. We work at that level of rigor for the ensemble theory.

Through this work, we demonstrate that several fundamental exact conditions from the ground-state theory hold for the ensemble theory but that others do not naturally carry over. We generalize coordinate scaling inequalities and equalities of the exchange and correlation energies and the concavity condition to ensembles. Although the logical steps are identical to those of ground-state theory (since both rely on the variational principle), the crucial point is that such steps and the resulting conclusions appear in this work. Using the Hubbard dimer, we show examples of each foundational condition and examine approximations in EDFT, finding examples of compliance and violation.

Figure 1 illustrates some of these conditions nicely [41]. It shows the limits (red) one can place on the $U = 5$ dimer (black) from results for $U = 4$ (blue), using one of our inequalities. The rest of this paper explains the behavior of these curves, including nonmonotonicity with weight and their shapes for large U. These exact results provide examples of the many ways in which EDFT can differ from ground-state DFT.

II. THEORY

A. Ensemble density functional theory

EDFT is a formally exact generalization of ground-state KS-DFT, where the ensemble consists of several eigenstates of an N-electron system. Consider any ensemble density matrix, $\hat{\Gamma}_w$, of the form

$$\hat{\Gamma}_w(\mathbf{r}_1 \dots \mathbf{r}_N, \mathbf{r}'_1 \dots \mathbf{r}'_N) = \sum_{m=0}^{M} w_m \left| \Psi_m(\mathbf{r}_1 \dots \mathbf{r}_N) \right\rangle \\ \times \left\langle \Psi_m(\mathbf{r}'_1 \dots \mathbf{r}'_N) \right|, \quad (1)$$
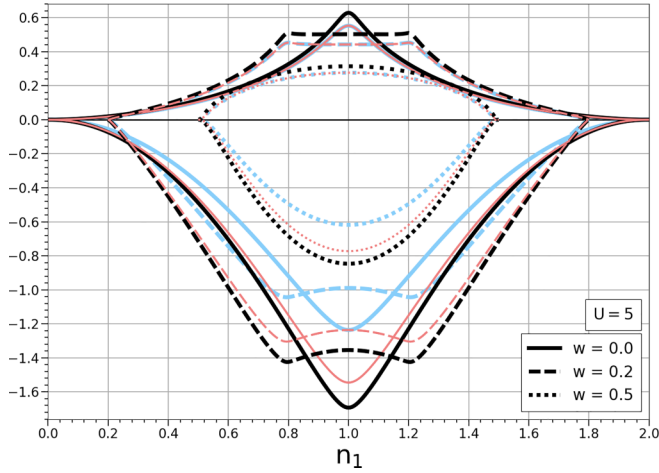
FIG. 1. The Hubbard dimer singlet bi-ensemble correlation energies (negative values) and kinetic contribution (positive values) for $U = 4$ (light blue) and $U = 5$ (black) as a function of site occupation and different weights. Red curves deduced from $U = 4$ constrain the $U = 5$ curve via Eq. (22).

where Ψ_m are any orthonormal wave functions, and w_m are positive, monotonically nonincreasing, and normalized weights. The expectation value of any operator $\hat{A}$ is then

$$A[\hat{\Gamma}_w] = \text{Tr}\{\hat{\Gamma}_w \hat{A}\} = \sum_{m=0}^{M} w_m \langle \Psi_m | \hat{A} | \Psi_m \rangle. \qquad (2)$$

An ensemble energy is then the variational minimum of the Hamiltonian, yielding the ensemble energy,

$$E_w = \min_{\hat{\Gamma}_w} \text{Tr}\{\hat{\Gamma}_w \hat{H}\}. \qquad (3)$$

Transition energies can be deduced from differences between ensemble calculations of differing weights [42]. EDFT tells us that there exists a w-dependent density functional

$$F_w[n] = \min_{\hat{\Gamma}_w \to n} \text{Tr}\{\hat{\Gamma}_w(\hat{T} + \hat{V}_{\text{ee}})\}, \qquad (4)$$

where $\hat{T}$ is the kinetic energy operator and $\hat{V}_{\text{ee}}$ is the electron-electron repulsion. We denote the minimizer by $\Gamma_w[n]$. Then

$$E_w = \min_n \left\{ F_w[n] + \int n(\mathbf{r}) v(\mathbf{r}) d\mathbf{r} \right\}, \qquad (5)$$

where $v(\mathbf{r})$ is the external potential.

Throughout this work, we use $A[\hat{\Gamma}]$ to denote a functional of $\hat{\Gamma}$, and also $A[n]$ to denote a density functional. These are two different functionals, as they have different arguments. However, one can convert a density matrix functional into a density functional, by defining:

$$A_w[n] = A[\hat{\Gamma}_w[n]], \qquad (6)$$

i.e., insertion of the unique, w-dependent minimizing density matrix for a given density into any functional of the density matrix creates a unique w-dependent ensemble density

functional. The minimizing density is

$$n_w(\mathbf{r}) = \sum_{m=0}^{M} w_m n_m(\mathbf{r}), \qquad (7)$$

where $n_m(\mathbf{r})$ is the density of the mth level.

A key facet of EDFT is that the equivalence between the exact density and the noninteracting KS density is only true for the ensemble average, and it is not generally true for the individual densities within the weighted sum. The following conditions are valid only for the ensemble energy, not the individual excited-state energies.

B. Exact conditions

Uniform coordinate scaling has been responsible for multiple advancements in DFT. However, coordinate scaling investigations in EDFT have thus far only been used to define the adiabatic connection formula for the exchange-correlation energy [40] or to examine the behavior of EDFT in the low-density and high-density regimes [39]. Additional work on foundational theorems include the virial theorem for EDFT by Nagy [43–45] and the signs of correlation energy components, by Pribram-Jones *et al.* [19]. We build on this foundation by deriving uniform scaling inequalities based on the variational definition of the ensemble functional [37,46]. We also provide numerical verification and proofs of the basic principles and some additional exact conditions.

We use norm-preserving homogeneous scaling of the coordinate $\mathbf{r} \to \gamma \mathbf{r}$ with $0 < \gamma < \infty$. The scaled density matrix is defined as

$$\Gamma_{w,\gamma}(\mathbf{r}_1 \dots \mathbf{r}_N') := \gamma^{3N} \Gamma_w(\gamma \mathbf{r}_1 \dots \gamma \mathbf{r}_N'), \qquad (8)$$

and a scaled density is $n_\gamma(\mathbf{r}) = \gamma^3 n(\gamma \mathbf{r})$. Trivially,

$$T[\Gamma_{w,\gamma}] = \gamma^2 T[\Gamma_w], \quad V_{\text{ee}}[\Gamma_{w,\gamma}] = \gamma V_{\text{ee}}[\Gamma_w]. \qquad (9)$$

Because these scale differently, $\Gamma_{w,\gamma}[n] \neq \Gamma_w[n_\gamma]$.

By the variational principle $F[n_{w,\gamma}] \leqslant F[\hat{\Gamma}_{w,\gamma}[n]]$, which gives the fundamental inequality of scaling,

$$T_w[n_\gamma] + V_{\text{ee},w}[n_\gamma] \leqslant \gamma^2 T_w[n] + \gamma V_{\text{ee},w}[n]. \qquad (10)$$

Manipulation of this formula yields [37],

$$T_w[n_\gamma] \leqslant \gamma^2 T_w[n], V_{\text{ee},w}[n_\gamma] \geqslant \gamma V_{\text{ee},w}[n], \gamma \geqslant 1$$

$$T_w[n_\gamma] \geqslant \gamma^2 T_w[n], V_{\text{ee},w}[n_\gamma] \leqslant \gamma V_{\text{ee},w}[n], \gamma \leqslant 1. \qquad (11)$$

Next, we turn to the KS scheme used in modern EDFT approaches. Here $F_w[n] = T_{\text{s},w}[n] + E_{\text{HXC},w}[n]$ where $T_{\text{s},w}$ is the KS kinetic energy and $E_{\text{HXC},w}$ is the Hartree-exchange-correlation. Because there is no interaction,

$$T_{\text{s},w}[n_\gamma] = \gamma^2 T_{\text{s},w}[n]. \qquad (12)$$

Moreover, because the Hartree exchange is linear in the scaling parameter:

$$E_{\text{HX},w}[n_\gamma] = \gamma E_{\text{HX},w}[n]. \qquad (13)$$

In EDFT, the separation of Hartree from the exchange is more complicated than in ground-state DFT [24,33,39].

Subtracting these larger energies following the usual procedure from ground-state DFT [37] yields

$$T_{c,w}[n_\gamma] \leqslant \gamma^2 T_{c,w}[n], \quad E_{c,w}[n_\gamma] \geqslant \gamma E_{c,w}[n], \quad \gamma \geqslant 1$$
$$T_{c,w}[n_\gamma] \geqslant \gamma^2 T_{c,w}[n], \quad E_{c,w}[n_\gamma] \leqslant \gamma E_{c,w}[n], \quad \gamma \leqslant 1, \quad (14)$$

where $E_{c,w}[n]$ is the correlation energy, and $T_{c,w} = T_w - T_{s,w}$ is its kinetic contribution. Considering $\gamma = 1 + \epsilon$ in Eq. (14), and taking $\epsilon \to 0$, yields differential versions of Eq. (14):

$$\frac{d}{d\gamma} \left\{ \frac{T_{c,w}[n_\gamma]}{\gamma^2} \right\} \leqslant 0, \quad \frac{d}{d\gamma} \left\{ \frac{E_{c,w}[n_\gamma]}{\gamma} \right\} \geqslant 0, \quad (15)$$

for all γ. Combining these using Nagy's generalization (Eq. (24) of Ref. [44]) of the ground-state equality

$$\frac{dE_{c,w}[n_\gamma]}{d\gamma} \bigg|_{\gamma=1} = E_{c,w}[n] + T_{c,w}[n], \quad (16)$$

we find

$$\frac{d^2}{d\gamma^2} \left\{ \frac{E_{c,w}[n_\gamma]}{\gamma} \right\} \leqslant 0, \quad (17)$$

or the condition for concavity in the ensemble correlation energy. Our first derivative conditions [Eq. (15)] are a generalization to ensembles of the ground-state result reported in Ref. [38]. That result is in fact a tighter bound than the original condition [Eq. (39) derived by Levy and Perdew in Ref. [47]]. Our concavity condition, Eq. (17), is the ensemble form of Eq. (40) in Ref. [47], but expressed more compactly as a function of γ.

Equations (10), (14), and (17) are primary results of the current work, being the ensemble generalizations of their ground-state analogs. An immediate application of Eq. (13) is to extract the HX component from any HXC approximation. As the conditions limit growth with γ,

$$E_{HX,w}[n] = \lim_{\gamma \to \infty} E_{HXC,w}[n_\gamma]/\gamma, \quad (18)$$

an exact condition that can prove useful for separating HX from C components [21,39].

To conclude this section, we use the pioneering relationship between coupling constant and coordinate scaling. Defining λ dependence via

$$F_w^\lambda[n] = \min_{\Gamma_w \to n} \text{Tr}\{\Gamma_w(\hat{T} + \lambda \hat{V}_{ee})\}, \quad (19)$$

Nagy showed [40]

$$E_{HXC,w}^\lambda[n] = \lambda^2 E_{HXC,w}[n_{1/\lambda}]. \quad (20)$$

Using Eq. (20), it is possible to rewrite all results given in terms of scaled densities as λ-dependent relations. Such relations are well known and extensively used in ground-state DFT via the adiabatic connection formalism [48,49]. For real-space Hamiltonians, these relations are simply a rewriting of the scaling relations in a more popular form, but they also apply to lattice Hamiltonians, where scaling is not possible. Converting from scaling in Eq. (16) gives

$$T_{c,w}^\lambda[n] = E_{c,w}^\lambda[n] - \lambda \frac{dE_{c,w}^\lambda[n]}{d\lambda}. \quad (21)$$

The scaling inequalities [Eqs. (14)] become

$$T_{c,w}^\lambda[n] \leqslant T_{c,w}[n], \quad E_{c,w}^\lambda[n] \geqslant \lambda E_{c,w}[n], \quad \lambda \leqslant 1,$$
$$T_{c,w}^\lambda[n] \geqslant T_{c,w}[n], \quad E_{c,w}^\lambda[n] \leqslant \lambda E_{c,w}[n], \quad \lambda \geqslant 1, \quad (22)$$

with differential versions

$$\frac{dT_{c,w}^\lambda[n]}{d\lambda} \leqslant 0, \quad E_{c,w}^\lambda[n] \geqslant \lambda \frac{dE_{c,w}^\lambda[n]}{d\lambda}, \quad (23)$$

while Eq. (17) becomes quite simply:

$$\frac{d^2 E_{c,w}^\lambda[n]}{d\lambda^2} \leqslant 0. \quad (24)$$

Note that all inequalities for $E_{c,w}$, both coordinate-scaled [Eqs. (14), (15)] and λ-dependent [Eqs. (22), (23)], are also true for the potential contribution to correlation $U_{c,w} = E_{c,w} - T_{c,w}$,

$$U_{c,w}^\lambda[n] \geqslant \lambda U_{c,w}[n], \quad \lambda \leqslant 1,$$
$$U_{c,w}^\lambda[n] \leqslant \lambda U_{c,w}[n], \quad \lambda \geqslant 1. \quad (25)$$

The HX energy [Eq. (18)] may be extracted via

$$E_{HX,w}[n] = \lim_{\lambda \to 0} E_{HXC,w}^\lambda[n]/\lambda. \quad (26)$$

Our last condition concerns the relationship between DFT and traditional approaches to quantum chemistry. In the ground state, it has long been known [50,51] that $0 \geqslant E_c^{HF} \geqslant E_c$, where E_c^{HF} is the traditional definition of the correlation energy, i.e., relative to the Hartree-Fock (HF) energy (we treat only restricted HF here, RHF). Given the complications of EDFT, we only discuss the case of the first singlet bi-ensemble for two electrons. In this case, we equate ensemble HF (EHF) with an EDFT EXX calculation (exact exchange only) [23]. The only difference between EHF and EDFT is that the EHF quantities are evaluated on the approximate EHF density, while EDFT quantities are evaluated on the exact density. The same variational reasoning leads us to

$$0 \geqslant E_{c,w}^{HF} \geqslant E_{c,w}[n], \quad (27)$$

where $E_{c,w}^{HF} = E_w - E_w^{HF}$, and E_w^{HF} minimizes $F_w = T_{s,w} + E_{HX,w}$. We leave the more general case to braver souls.

C. Hubbard dimer model

To illustrate these exact conditions, we use the Hubbard dimer model, which can be solved analytically. The Hamiltonian of the Hubbard dimer is

$$\hat{H} = -t \sum_\sigma (\hat{c}_{1\sigma}^\dagger \hat{c}_{2\sigma} + \text{h.c.}) + U \sum_i \hat{n}_{i\uparrow} \hat{n}_{i\downarrow} + \sum_i v_i \hat{n}_i, \quad (28)$$

where t is the hopping parameter, U the on-site electrostatic self-repulsion, and v_i the on-site potential (which controls the asymmetry of the dimer). For this lattice system, with $N = 2$, the electronic density is characterized by a single number, the difference between occupations of the two sites, $\Delta n = n_2 - n_1$. The λ dependence of any quantity is found by replacing U by λU, keeping Δn fixed. We choose $t = 1/2$ everywhere.

We consider the simplest bi-ensemble, a mixture of the ground state with the first excited singlet. Full analytic expressions of $|\Psi_0\rangle$ and $|\Psi_1\rangle$, as well as plots of various bi-ensemble
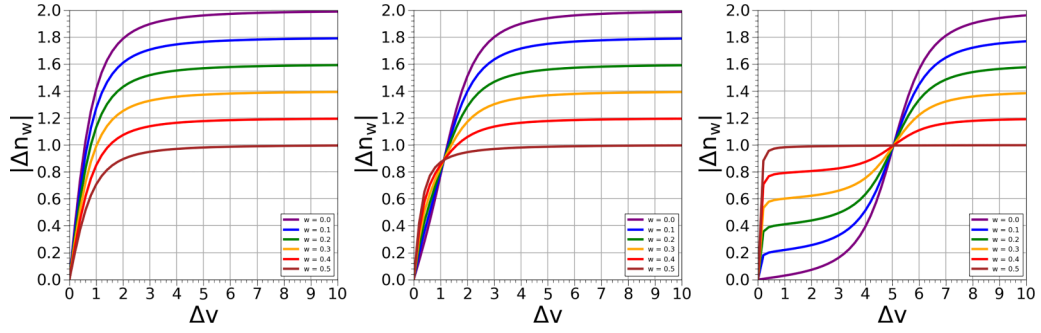
FIG. 2. Absolute value of the density of the Hubbard dimer bi-ensemble, plotted for various weight values as a function of Δv. Here we set $U = 0$ (left), $U = 1$ (center), and $U = 5$ (right).

quantities are included in the Appendix. The value of Δn_w is constrained by w:

$$|\Delta n_w| \leqslant 2\overline{w}, \qquad (29)$$

where $\overline{w} = 1 - w$, i.e., is smaller than that of the ground state ($w = 0$).The total energy of the ensemble is defined as

$$E_w = \overline{w} \langle \Psi_0 | \hat{H} | \Psi_0 \rangle + w \langle \Psi_1 | \hat{H} | \Psi_1 \rangle. \qquad (30)$$

For this bi-ensemble, the exact HX energy has the simple analytical form [23]:

$$E_{\text{HX},w} = \frac{U}{2} \left[1 + w + \frac{(1 - 3w)}{\overline{w}^2} \frac{\Delta n_w^2}{4} \right]. \qquad (31)$$

The density of each state is trivially $\Delta n_i = 2[(\beta_i^-)^2 - (\beta_i^+)^2]$, with $\beta_i^\pm$ reported in the Appendix, meaning that the ensemble density is

$$\Delta n_w = 2\overline{w}[(\beta_0^-)^2 - (\beta_0^+)^2] + 2w[(\beta_1^-)^2 - (\beta_1^+)^2], \qquad (32)$$

where $\overline{w} = 1 - w$. Plots of this difference are included in Fig. 2 for three interaction strengths, $U = 0$, 1, and 5.

Analyzing this figure, it is clear that there are vast differences in the behavior of Δn_w with respect to the value of U, illustrating the importance of developing weight-dependent approximations for electronic correlation. Two characteristics are present in all plots of Δn_w, these being an adherence to the symmetric limit ($\Delta v = \Delta n_w = 0$) and a maximum value constraint imposed by the representability condition $|\Delta n_w| \leqslant 2\overline{w}$, which each curve approaches as $\Delta v \to \infty$.

As predicted by EDFT in Eq. (32), the density is linear in w. For sufficiently large U, there exists a value of Δv at which the initial slope of the first excited state density difference is negative. Still, it always becomes positive for sufficiently large Δv. Thus, there is a specific value of Δv at which the first excited state density vanishes, and all curves meet at that point, independent of w. This point tends to $\Delta v = U$ as U becomes large.

For finite values of U, a trend in curve steepness with respect to the weight is evident for small Δv; the steepness of each curve is directly proportional to the value of w, signifying that ensembles with larger w values approach their maximum value more quickly. The severity of steepness increases drastically as U is increased, as shown by the behavior of the $U = 5$ curves as $\Delta v \to 0$. Here, the densities increase rapidly to $|\Delta n_w| \approx 2w$, becoming nearly perfectly antisym-

metric around $\Delta v = U$, with a very sharp dive to 0 for very small Δv. It also appears that all Δn_w curves approach the same value at $\Delta v \approx U$ as $U \to \infty$. As $U \to \infty$ the density forms a step function, flipping from $2w$ to $2\overline{w}$ at $\Delta v = U$.

The correlation energies are then found by using the exact expressions:

$$T_{\text{c},w} = T_w - T_{\text{s},w}, \qquad (33)$$

$$U_{\text{c},w} = V_{\text{ee},w} - E_{\text{HX},w}, \qquad (34)$$

$$E_{\text{c},w} = T_{\text{c},w} + U_{\text{c},w}. \qquad (35)$$
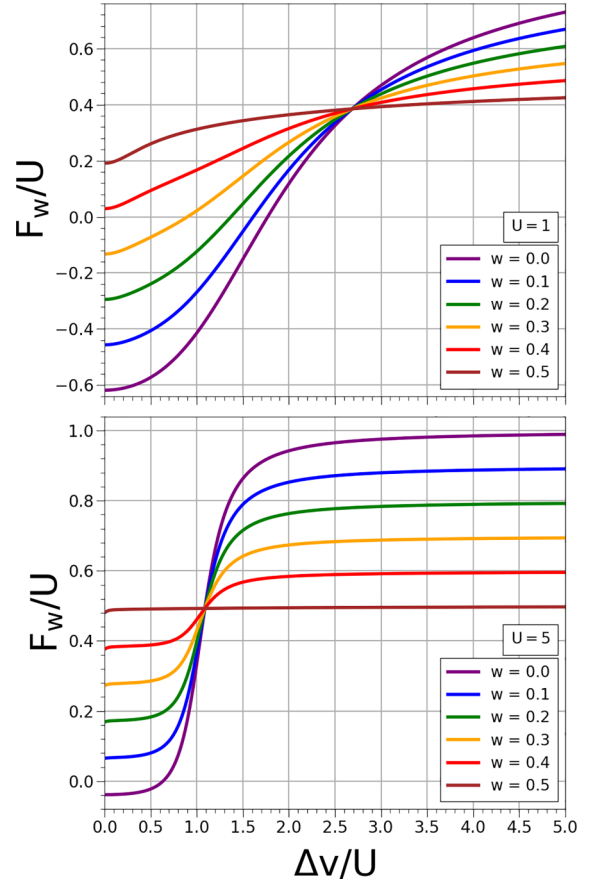
FIG. 3. F_w/U of the Hubbard dimer bi-ensemble plotted as a function of Δv for various w values. Here we set $U = 1$ (top) and $U = 5$ (bottom).

FIG. 4. F_w/U of the Hubbard dimer bi-ensemble plotted as a function of Δn_w for various w values. Here we set $U = 1$ (top) and $U = 5$ (bottom).
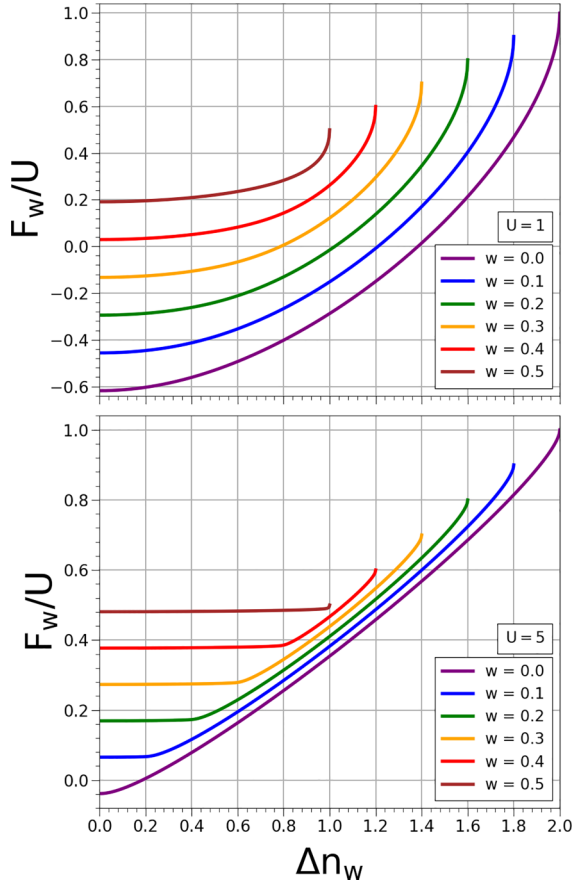
FIG. 5. $E_{\mathrm{HXC},w}/U$ of the Hubbard dimer bi-ensemble plotted as a function of Δn_w for various w values. Here we set $U = 1$ (top) and $U = 5$ (bottom).

We also examine the properties of the Hubbard dimer equivalent of the universal part of the density functional, $F_w = E_w - \Delta v \Delta n_w/2$, plotting again as a function of Δv and Δn_w in Figs. 3 and 4, respectively. In Fig. 3, one can see that F_w is linear with respect to bi-ensemble weight when plotted as a function of Δv. This characteristic is not present in Fig. 4, where monotonicity is broken as $\Delta n_w \to 2\overline{w}$. Furthermore, as U is increased, one can see the appearance of regimes around $\Delta n_w = 2w$, with F_w being nearly independent of Δn_w for $\Delta n_w < 2w$ and linearly increasing as $\Delta n_w > 2w$. Additionally, the curves depicting F_w tend to flatten as w increases.

In contrast, we plot $E_{\mathrm{HXC},w}$ in Fig. 5 and see it is nonmonotonic in w. The curvature of $E_{\mathrm{HXC},w}$ changes from convex to concave as the weight increases, and the $E_{\mathrm{HXC},w}$ curves cross each other at various points, with the most noticeable crossings happening at $U = 1$. However, the curves cross at all the values of U plotted. We conclude that curves become nonmonotonic when plotted as a functional of the density instead of the potential, as the curves of Fig. 2 are certainly not monotonic.

For fixed Δv, Fig. 6 illustrates that E_w is correctly linear in w. The curves are uninteresting for $U = 1$ but develop a pinch around $\Delta v = U$ as U grows larger. However, Fig. 7 shows that, as a functional of Δn, the curves are no longer linear in w. They are not even monotonic, as $\Delta n_w \to 2\overline{w}$, $E_w \to -\infty$, the curves cross. Interesting behavior also exists

as U is increased, with E_w becoming ever more slowly varying with density for $\Delta n_w < 2w$. This behavior may be explained through the relationship between Δn_w and Δv shown in the right panel of Fig. 2, where there is a drastic change in Δn_w for $\Delta v \approx 0$.

III. RESULTS

In this section, we examine all the exact conditions within the context of the Hubbard dimer model. We also extend our analysis to the strongly correlated regime and quantum chemistry analogies.

A. Inequalities

First, we examine the correlation inequalities [Eq. (22)]. We highlight in Fig. 8 the definite signs of the correlation energy and its components. This illustrates results initially introduced by Pribram-Jones *et al.* [19].

Looking at Figs. 9 and 10, one can see that the correlation inequalities of Eq. (22) are satisfied for all values of Δn_w. There is a clear trend for the weight for the symmetric dimer: the ground state has the maximum magnitude in each plot and then decreases in magnitude with an increase in w. So for the symmetric dimer ($\Delta n_w = 0$), $w = 0$ has the largest maximum, and $w = 0.5$ has the smallest. This trend no longer
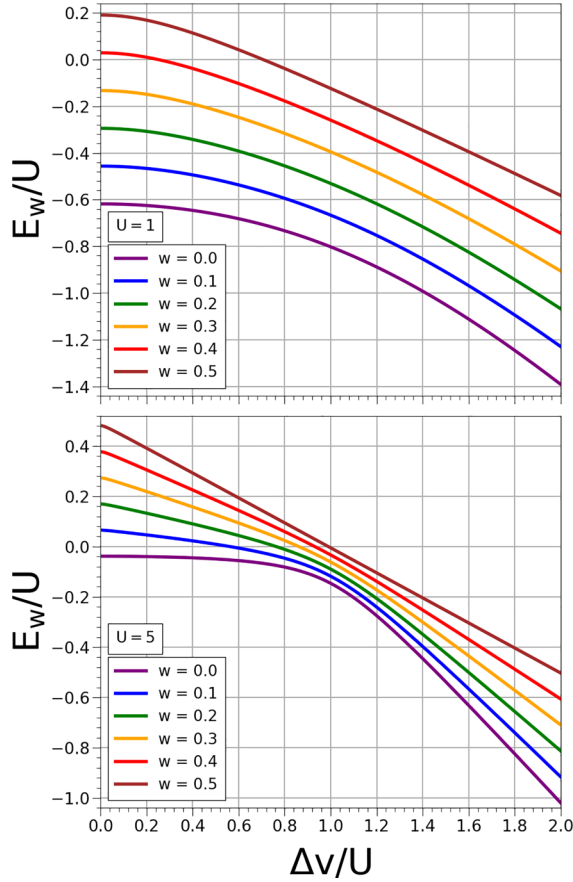
FIG. 6. Total energy of the Hubbard dimer bi-ensemble plotted as a function of Δv for various w values. Here we set $U = 1$ (top) and $U = 5$ (bottom).

FIG. 7. Total energy of the Hubbard dimer bi-ensemble plotted as a function of Δn_w for various w values. Here we set $U = 1$ (top) and $U = 5$ (bottom).

holds for $\Delta n_w \neq 0$. Alternative approaches were implemented in which Δv was held fixed, again showing no clear trend for asymmetric dimers. Furthermore, the inequalities of Eq. (22) become equalities as $\Delta n_w \to 2\overline{w}$, explaining the flat behavior of the $w = 0.5$ curves for $\Delta n_w = 1$. The shape of all curves depends strongly on U.

B. Adiabatic connection

We now examine the adiabatic connection curves in Fig. 11. First, we note that many curves look similar to ground-state DFT and are monotonically decreasing and are convex. However, as Δn_w increases, the curves vary less with λ. For nonzero Δn_w, concave regions appear when $w > 1/3$. Such concave curvature has not been observed in ground states in the Hubbard dimer [52,53] and is only observed in the ensemble framework as more weight is placed on the excited state. This offers an interesting counterexample to the convexity of the adiabatic connection, which is still an open question in density functional theory [54]. Convexity of the adiabatic connection has never been proven, and our example makes it unlikely to be true for ensembles. We also note that the convexity in the adiabatic connection curve is not equivalent to the concavity condition for the correlation energies, Eq. (24).
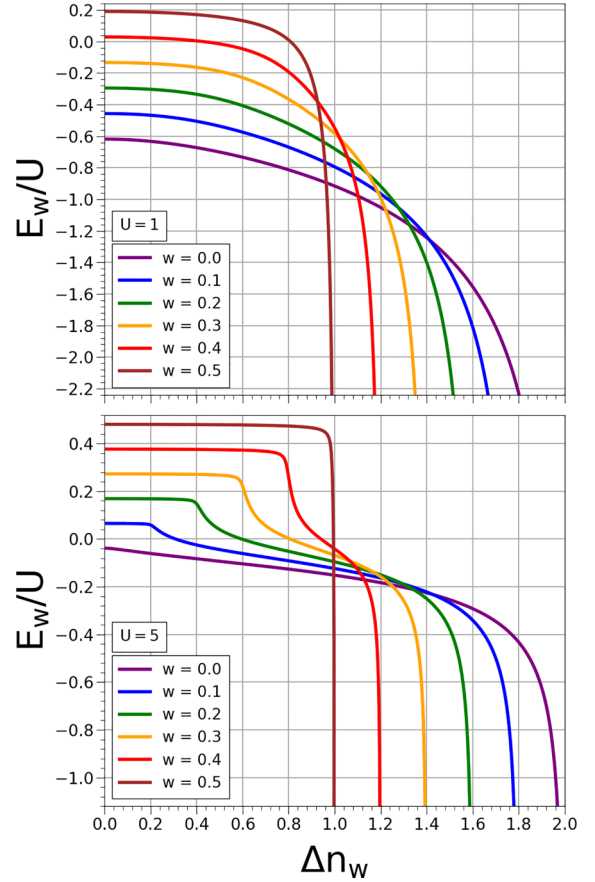
In Fig. 11, we also observe an interesting change in the ordering of the HX energy values based on the weights. For $\Delta n_w < 0.6$, the HX energy monotonically decreases as the weights increase and the spacing between the values shrinks. However, after that point, the ordering shifts and the $w = 0.5$ weight has the maximum HX value. Additionally, as $\Delta n_w \to 1$, and $\lambda \to \infty$, the value of the HXC expression becomes w independent. We also show that all $U_{\text{HXC},w}$ curves approach their corresponding HX value as $\lambda \to 0$, in accordance with Eq. (26). The nonmonotonic behavior in Fig. 1 can be easily understood. By definition, $E_w(\Delta v)$ is linear in w, as is F_w. But,
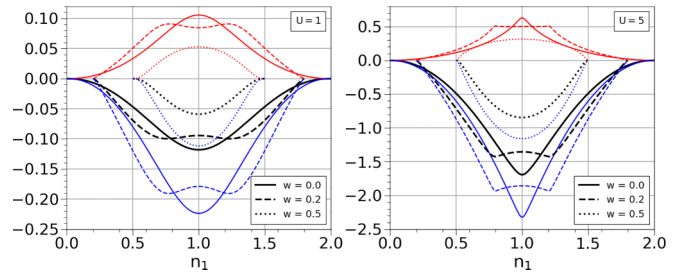
FIG. 8. Variation of the potential (blue), kinetic (red), and total (black) correlation energies in the Hubbard dimer bi-ensemble, plotted as functions of site-occupation of the first site for various weights. We set $U = 1$ on the left and $U = 5$ on the right.
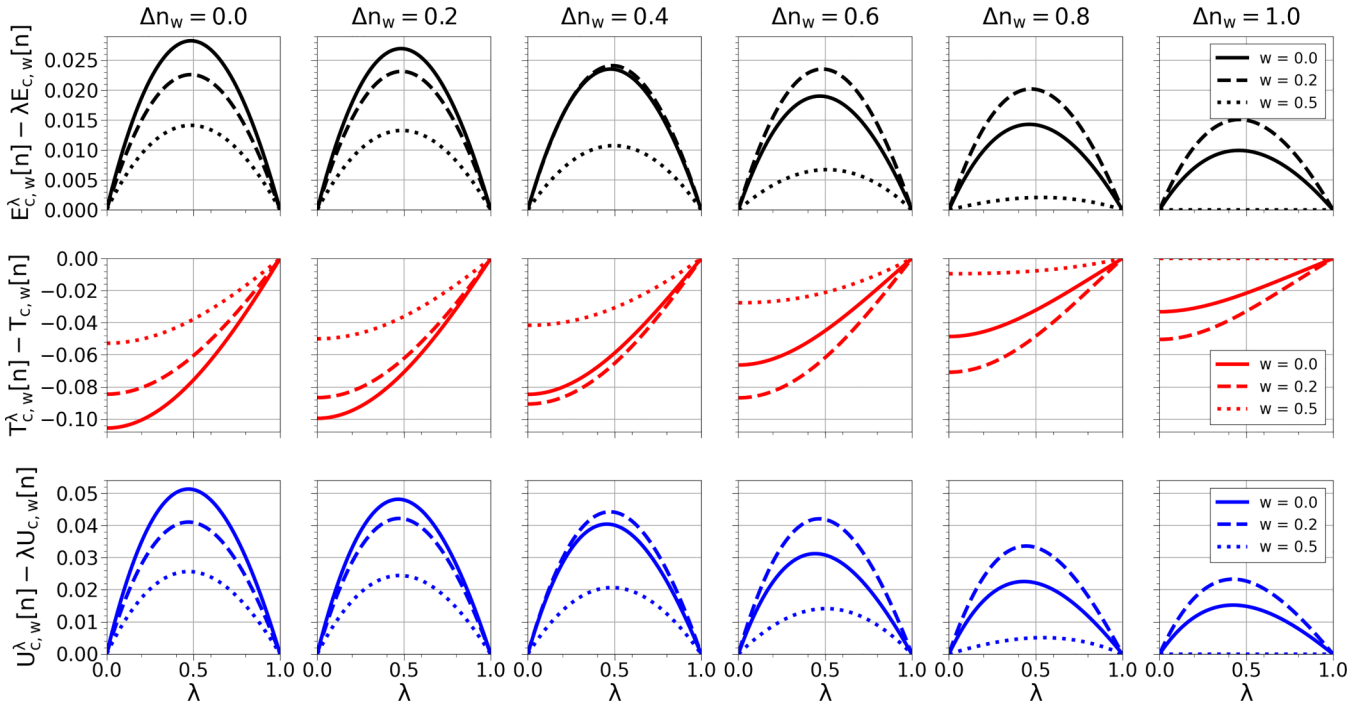
FIG. 9. Correlation inequalities [Eq. (22)] for the total (top), kinetic (middle), and potential (bottom) correlation energies, depicted by varying λ in the Hubbard dimer bi-ensemble with $U = 1$.

when converted to density functionals, and with KS quantities subtracted, these become highly nonmonotonic. Moreover, Fig. 12 demonstrates that the convexity conjecture [54] for the ensemble adiabatic connection curve is not generally satisfied.

This condition is only postulated for the ground-state case. Unlike Eq. (24), the convexity conjecture of the adiabatic connection curve is a stronger conjecture related to the third λ derivative of $E_{c,w}^{\lambda}[n]$.
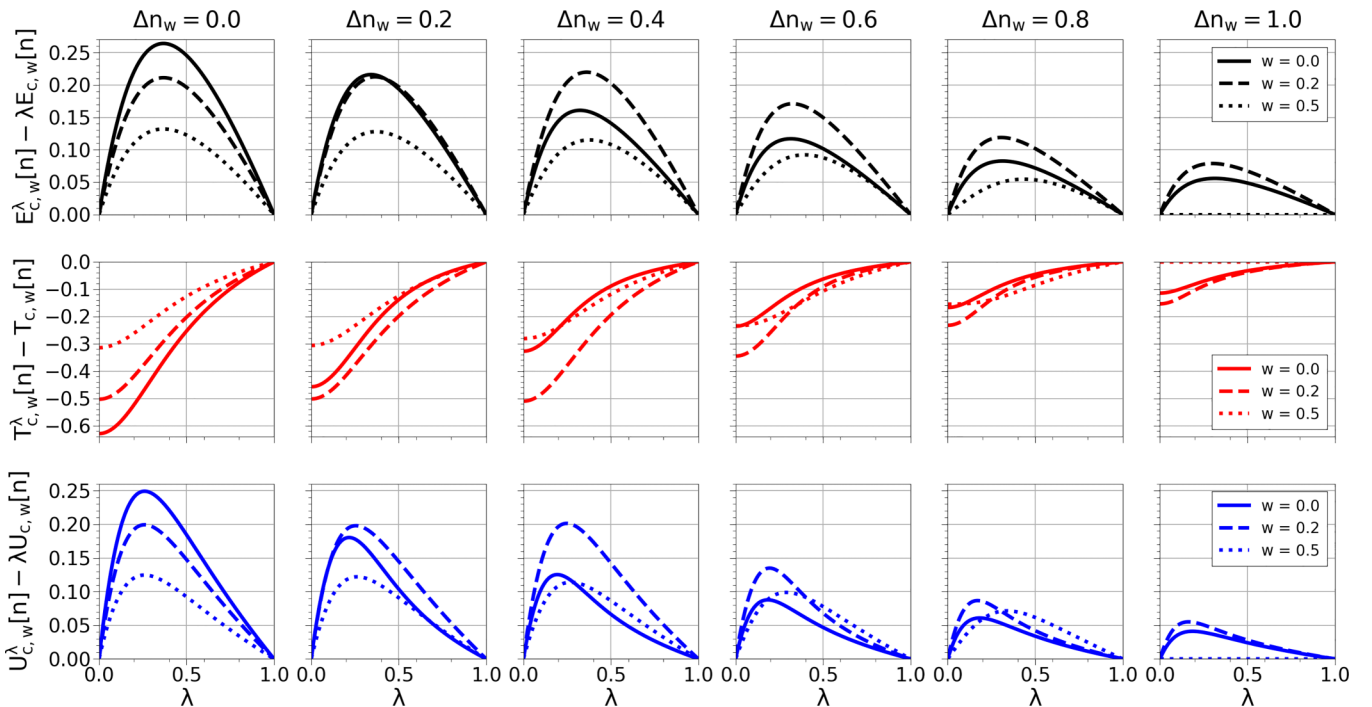
FIG. 10. Correlation inequalities [Eq. (22)] for the total (top), kinetic (middle), and potential (bottom) correlation energies, depicted by varying λ in the Hubbard dimer bi-ensemble with $U = 5$.
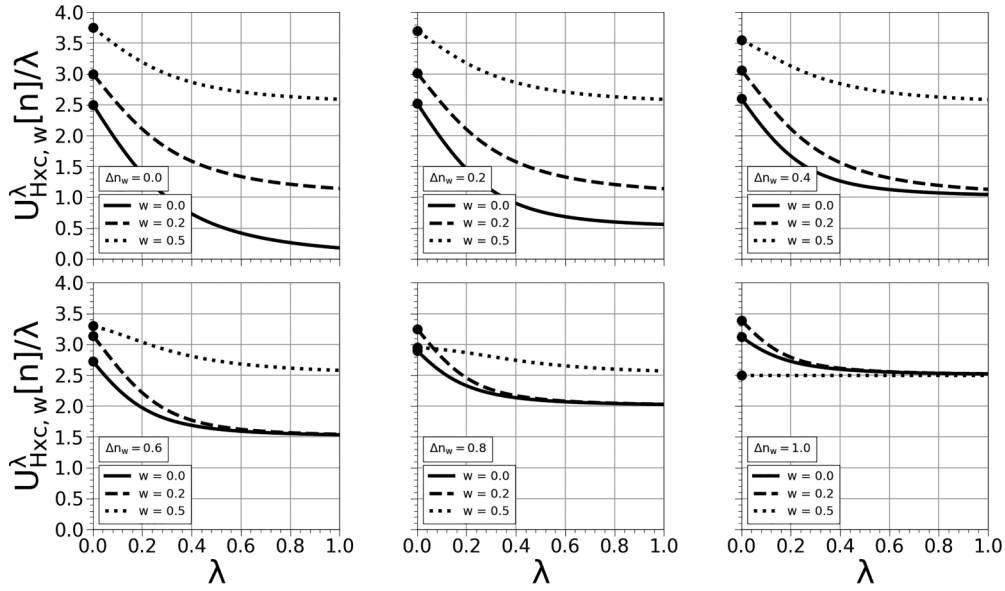
FIG. 11. Ensemble adiabatic connection for $U = 5$ and various Δn_w; circles represent the weight-dependent HX energy, which the HXC expression approaches as $\lambda \to 0$.

C. Concavity condition of the correlation energy

We illustrate the concavity condition of Eq. (24) using contour plots depicting all possible combinations of U and n_1, making use of the reduced variable $\tilde{u} = U/\sqrt{1+U^2}$. Illustrated by Fig. 13, the second derivative is negative for all values of U, thus satisfying the concavity condition for all electronic correlation strengths. The standard use of exact conditions in DFT is to ensure that approximate functionals satisfy them [38]. We illustrate our conditions by applying them to existing approximations on the Hubbard model. The first is the standard many-body expansion in powers of the interaction, U, which we perform up to second order, i.e., the analog of Møller-Plesset perturbation theory, denoted U-PT2 (not shown in Fig. 13). The second is less familiar: an expansion in powers of Δn around the symmetric case, $\Delta n = 0$,

called δ-PT2 [55]. This can be considered a (tortured) analog of the gradient expansion of DFT [36], as it is an expansion around the uniform limit. Figure 13 shows that the δ-PT2 approximation violates the concavity condition, even for $w = 0$, while U-PT2 never does by construction. The violations are not monotonic with increasing weights, as $w = 0.4$ has none. Deur *et al.* reported that, compared to U-PT2, δ-PT2 produced more accurate equi-ensemble energies and densities. Likely, the accuracy of δ-PT2 could be further improved by imposing concavity. Recent advances in EDFT, such as the direct ensemble correction [20] and the perturbative EDFT method [56], are explicitly computed in the perturbative limit, $w \to 0^+$. If an approximation is derived before such a limit is taken, and its ground-state approximation satisfies concavity; the resulting approximation should satisfy concavity also.

D. Strong correlation

We now examine the behavior of the Hubbard dimer in the strongly correlated regime. For fixed w, as U becomes large, one can keep Δv fixed or $\Delta v/U$ fixed. The former was explored by Deur *et al.* [55] and produces the pale blue curves of Fig. 14. As the figure shows, the blue curves yield the correct answer only for $|\Delta n_w| \leqslant 2w$, which shrinks to a point as $w \to 0$.

The appropriate expansion to find $E_{c,w}(\Delta n)$ for large U and $|\Delta n| > 2w$ is shown in the red curves. We take $U \to \infty$ but keep $\Delta v/U$ fixed. This step is required to include values of Δn away from $\Delta n \approx 0$ while including all allowed values of Δn. The strongly correlated limit of Ref. [55] can be recovered from our limit by expressing the Δv dependence explicitly and taking $U \to \infty$; this no longer keeps the ratio $\Delta v/U$ fixed. A careful expansion yields the total energy as a function of $x = \Delta v/U$:

FIG. 12. The second derivative of the ensemble adiabatic connection with respect to λ for $U = 5$ and $\Delta n_w = 0.9$.

$$E_w(x) \to U\left(g_w^{(0)}(x) + \frac{g_w^{(2)}(x)}{U^2} + \cdots\right), \qquad (36)$$
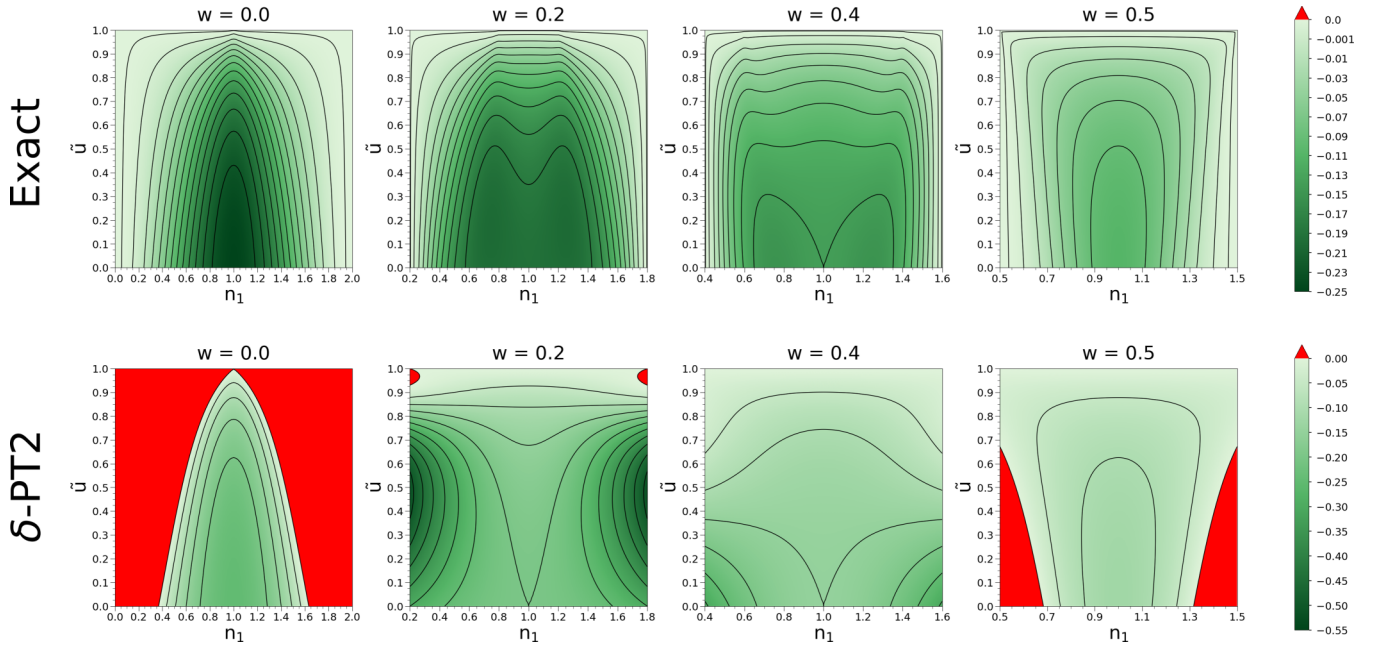
FIG. 13. The second derivative of the Hubbard dimer bi-ensemble correlation energy with respect to U for all values of the reduced variable $\tilde{u} = U/\sqrt{1+U^2}$. The concavity condition is satisfied exactly, but is violated by the δ-PT2 approximation in certain regimes (red denotes positive). U-PT2 automatically satisfies the concavity condition by construction.

where

$$g_w^{(0)}(x) = \frac{1}{3}(2 - (c - \sqrt{3}s)h) - \frac{2shw}{\sqrt{3}}, \qquad (37)$$

and

$$g_w^{(2)}(x) = \frac{1}{2h}\left(\frac{(\alpha - 3)s}{\sqrt{3}} - (\alpha + 1)c\right) + \frac{1}{h}(\alpha c + \sqrt{3}s)w, \qquad (38)$$
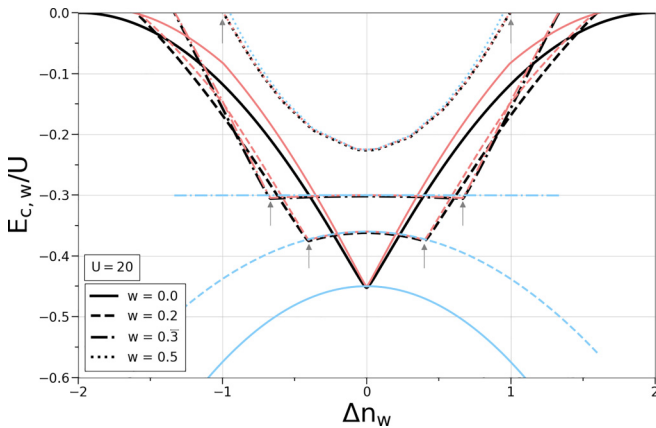
FIG. 14. Exact correlation energy (black), leading-order expansion in large U (red), and the expansion in the symmetric limit (blue) for the correlation energy are all plotted as a function of the exact density. Small arrows indicate the region between $2w$ and $-2w$ where the symmetric expansion matches the exact.

where $\alpha = |4x/(x^2 - 1)|$, $c = \cos(\phi)$, and $s = \sin(\phi)$ with,

$$\phi = \frac{1}{3}\cos^{-1}\left(\frac{3h^2 - 4}{h^3}\right), \quad h = \sqrt{3x^2 + 1}. \qquad (39)$$

The angle ϕ is positive for all values of x, where it takes its maximal value of $\pi/3$ as $x \to 0$ and minimal value of 0 as $x \to \pm 1$, and in the limit $\phi(x \to \pm\infty) = \pi/6$. Because the angle is constrained to $0 \leqslant \phi \leqslant \pi/3$, the sine and cosine must be $0 \leqslant c, s \leqslant \sqrt{3}/2$.

The corresponding density is found via $\Delta n_w = 2dE_w/d(\Delta v)$,

$$\Delta n_w(x) = 2\left(g_w^{(0)\prime}(x) + \frac{g_w^{(2)\prime}(x)}{U^2} + \cdots\right), \qquad (40)$$

where primes denote derivatives with respect to x. Retaining only zero-order terms yields,

$$g_w^{(0)\prime}(x) = \frac{1}{h}\left(\frac{(\gamma - 3x)s}{\sqrt{3}} - (\gamma + x)c\right) + \frac{2}{h}(\gamma c + \sqrt{3}xs)w, \qquad (41)$$

with $\gamma = \text{sgn}[x(1 - x^2)]$. Because the expansion in U is singular near $x = 0$ and $x = \pm 1$, $g_w^{(2)}(x)$ diverges at $|x| = 1$, and even $n_w^{(0)}(x) = 2g_w^{(0)\prime}(x)$ contains discontinuous steps. While formally correct in the limit $U \to \infty$, the exact density cannot have such steps due to the Hohenberg-Kohn theorems. We therefore smooth Eq. (41) with exponentials that become infinitely sharp as $U \to \infty$:

$$\Delta n_w \approx \frac{x}{|x|}(f(|x|) - 1)\left(1 + (1 - 2w)\tanh\left(\frac{\beta(|x| - 1)}{2}\right)\right), \qquad (42)$$
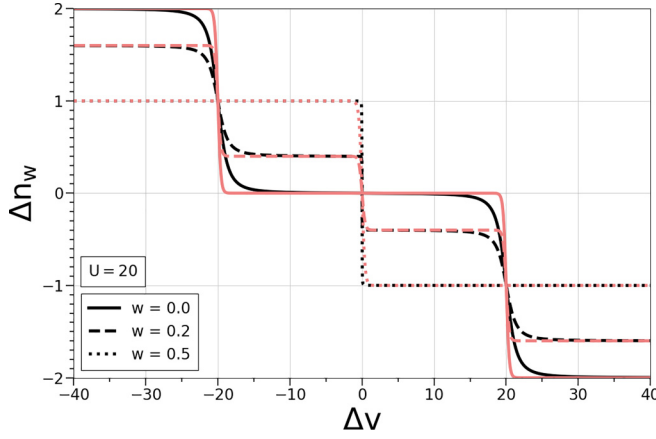
FIG. 15. Smooth approximation for the density Eq. (42) (light red) and the exact density (black) Eq. (32) plotted against Δv.

where $f(x) = [\exp(\beta x) + 1]^{-1}$ is the Fermi-Dirac distribution with $\beta = 5U$. This is plotted in Fig. 15 and is compared with the exact density. As $U \to \infty$, Eq. (42) matches Eq. (41).

Using our leading-order density in Eq. (41) and the next higher-order correction to the ensemble energy in Eq. (36), we derive the strongly correlated expansion of the universal part of the energy functional,

$$F(\Delta n_w(x)) = U\left(g_w^{(0)}(x) - \frac{x\Delta n_w(x)}{2}\right) + \frac{g_w^{(2)}(x)}{U}. \quad (43)$$

Finally, we subtract the remaining components to determine the correlation energy:

$$E_{c,w}(\Delta n_w(x)) \approx U\left(g_w^{(0)}(x) - \frac{x\Delta n_w(x)}{2}\right) - E_{HX,w}(\Delta n_w(x))$$
$$- T_{s,w}(\Delta n_w(x)) + \frac{g_w^{(2)}(x)}{U}. \quad (44)$$

Including only the lowest order and inserting the smooth density, Eq. (42), yields the plot in Fig. 14, and the curves in Fig. 15. We also plot the next order contribution to the correlation energy, Eq. (44), in Fig. 16. To avoid divergences from α at $x = \pm 1$, we use a smooth approximation to the absolute values that appear in the denominator of Eq. (38).

In Fig. 14, we plot the exact correlation energy, our approximation [Eq. (44)], and the symmetric limit expansion of Deur *et al.* [55], each evaluated at the exact density. The expansion about the symmetric limit correctly produces the strongly correlated correlation energy, but only for $|\Delta n_w| \leqslant 2w$, as expected by its derivation. Our expansion yields the correct limit for all allowed Δn_w, including the slope discontinuity at $|\Delta n_w| = 2w$. Such w-dependent derivative discontinuities occur only in EDFT.

The approximate weight-dependent strongly correlated correlation energy along the density-functional adiabatic connection is derived along with further analysis of the energy components and approximation of the density. For the strong-interaction limit of the dimer, the correlation energy contains nontrivial weight dependence. This differs from the real-space continuum case [39] where the energies are known to be weight independent. This is not a counterexample to that case
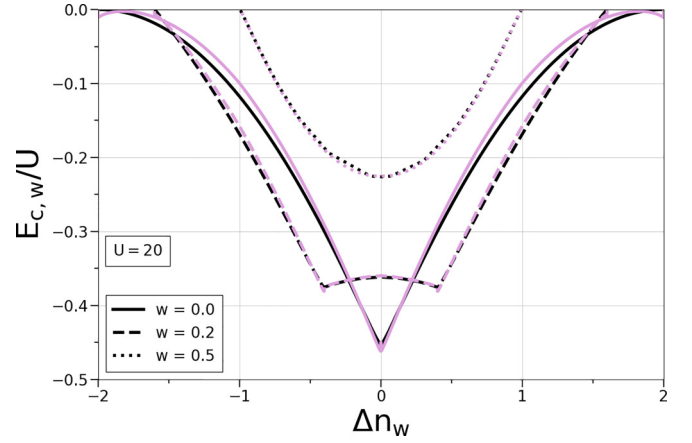
FIG. 16. The exact (black) correlation energy as a function of the exact density and our higher-order expansion in large U (light purple) for the correlation energy Eq. (44), plotted as a function of the smooth approximation for the density Eq. (42).

because the dimer is a site model. This difference is apparent in the expansion of the strongly correlated energies in powers of the coupling constant. Our first correction [Eq. (43)], relative to the leading term, is $\mathcal{O}(\lambda^{-2})$ and differs qualitatively from the $\mathcal{O}(\lambda^{-1/2})$ behavior in the continuum.

We produce an expression for $E_{c,w}^{\lambda}(\Delta n_w)$ where Δn_w is kept fixed for each λ along the adiabatic connection. For sufficiently large U we neglect all terms of $\mathcal{O}(1/U^2)$ and lower. In this limit, $\Delta n_w(x) \to \Delta n_w^{(0)}(x)$, and by the adiabatic connection construction we have the requirement that $\Delta v/U \approx \Delta v^{\lambda}/(\lambda U)$, where Δv^{λ} is the λ-dependent potential that keeps Δn_w fixed along the connection. As a consequence, to leading order,

$$\Delta v^{\lambda}(\Delta n_w) \approx \lambda \Delta v^{(0)}(\Delta n_w), \quad (45)$$

and thus,

$$E_w^{\lambda}(\Delta n_w) \approx \lambda U g_w^{(0)}(x^{(0)}(\Delta n_w)) + \frac{g_w^{(2)}[x^{(0)}(\Delta n_w)]}{\lambda U}, \quad (46)$$

where $x^{(0)}(\Delta n_w) = \Delta v^{(0)}(\Delta n_w)/U$ is the inversion of the leading-order density-potential map, Eq. (45). The universal part of the functional is found by subtracting the external potential energy from Eq. (46),

$$F_w^{\lambda}(\Delta n_w) \approx \lambda U\left(g_w^{(0)}(x^{(0)}(\Delta n_w)) - \frac{x^{(0)}(\Delta n_w)\Delta n_w}{2}\right)$$
$$+ \frac{g_w^{(2)}(x^{(0)}(\Delta n_w))}{\lambda U}. \quad (47)$$

To produce the correlation energy we subtract from Eq. (47) the KS kinetic energy [Eq. (A3)] and the HX energy [Eq. (A4)],

$$E_{c,w}^{\lambda}(\Delta n_w) \approx \lambda U\left(g_w^{(0)}(x^{(0)}(\Delta n_w)) - \frac{x^{(0)}(\Delta n_w)\Delta n_w}{2}\right.$$
$$\left. - e_{Hx,w}(\Delta n_w)\right) - T_{s,w}(\Delta n_w)$$
$$+ \frac{g_w^{(2)}(x^{(0)}(\Delta n_w))}{\lambda U}, \quad (48)$$
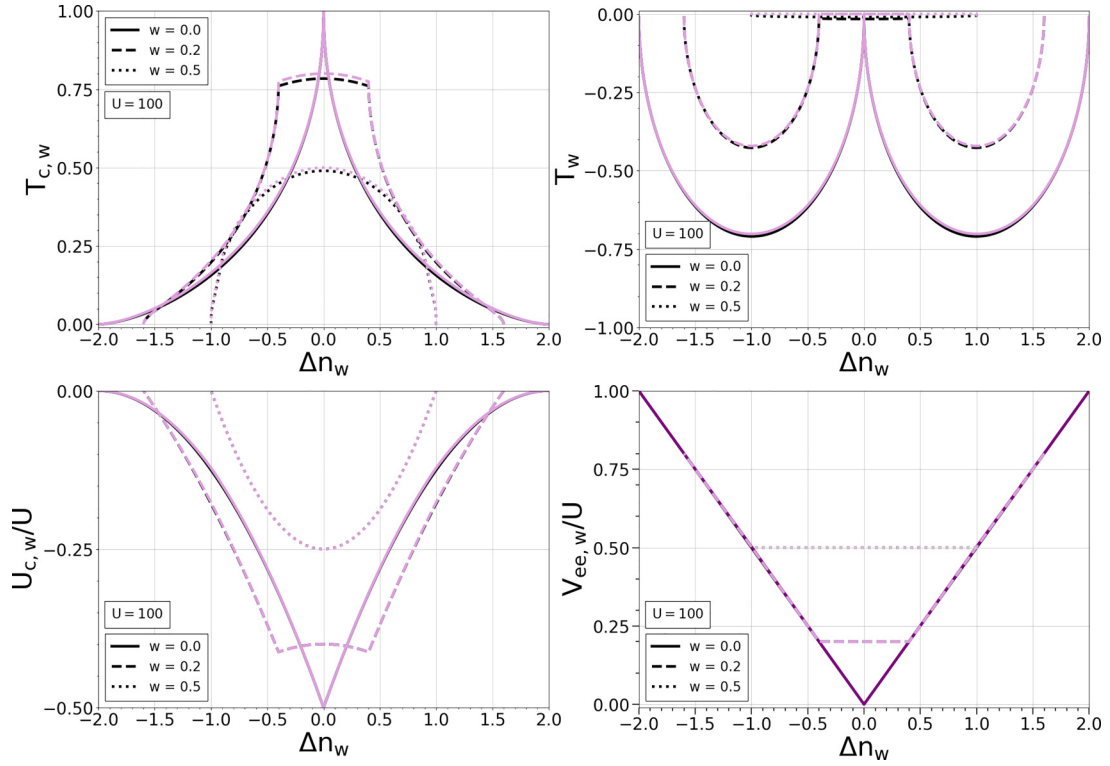
FIG. 17. $T_{c,w}$, Eq. (49), $U_{c,w}$, Eq. (50), T_w, Eq. (51), and $V_{ee,w}$, Eq. (52) for various values of w and $U = 100$. The exact values in the strongly correlated limit are represented by the black curves, which are exact as $U \to \infty$.

where Δn_w remains fixed for all λ and $e_{Hx,w}(\Delta n_w) = E_{Hx,w}(\Delta n_w)/U$.

Equation (21) yields expressions for the separate kinetic and potential contributions to the correlation energy,

$$T_{c,w}(\Delta n_w) \approx \frac{2g_w^{(2)}(x^{(0)}(\Delta n_w))}{U} - T_{s,w}(\Delta n_w), \qquad (49)$$

$$U_{c,w}(\Delta n_w) \approx U\left(g_w^{(0)}(x^{(0)}(\Delta n_w)) - \frac{x^{(0)}(\Delta n_w)\Delta n_w}{2}\right. \\ \left. - e_{Hx,w}(\Delta n_w)\right) - \frac{g_w^{(2)}(x^{(0)}(\Delta n_w))}{U}. \qquad (50)$$

From the separate contributions of the correlation energy, we deduce that,

$$T_w(\Delta n_w) \approx \frac{2g_w^{(2)}(x^{(0)}(\Delta n_w))}{U}, \qquad (51)$$

$$V_{ee,w}(\Delta n_w) \approx U\left(g_w^{(0)}(x^{(0)}(\Delta n_w)) - \frac{x^{(0)}(\Delta n_w)\Delta n_w}{2}\right) \\ - \frac{g_w^{(2)}(x^{(0)}(\Delta n_w))}{U}. \qquad (52)$$

We plot Eqs. (49)–(52) in Fig. 17 with the exact expressions in black and the approximate expressions evaluated with the smooth density in purple. In all plots, we use the same smooth approximation to the absolute values in the denominators of

$g_w^{(2)}(x)$. The errors in the plots of the correlation kinetic energy vanish as $U \to \infty$.

We compare our result in Eq. (44), for $|\Delta n_w| \leqslant 2w$, with the symmetric limit expansion of Deur *et al.* [55]. To properly compare our approximate correlation energy to the previously reported expansion in the symmetric limit, we produce the weight-dependent constant that vanishes in the limit $U \to \infty$,

$$\frac{E_{c,w}(\Delta n_w)}{U} \approx \frac{\overline{w}}{U} - \frac{1}{2}\left(\overline{w} - \frac{(3w-1)}{\overline{w}^2}\frac{\Delta n_w^2}{4}\right), \qquad (53)$$

which is derived following the procedure in Ref. [55].

E. Quantum chemistry

Finally, we examine the difference between the DFT and HF correlation energies and their components in detail. Our HF definition is based on a weighted sum of ground- and excited-state Coulomb-exchange energies [28,34]. We define the Hartree-Fock solution of each state [analogous to Eq. (A2)] to be

$$|\Phi_i\rangle = \alpha_i^{HF}(|12\rangle + |21\rangle) + \beta_i^{+HF}|11\rangle + \beta_i^{-HF}|22\rangle, \qquad (54)$$
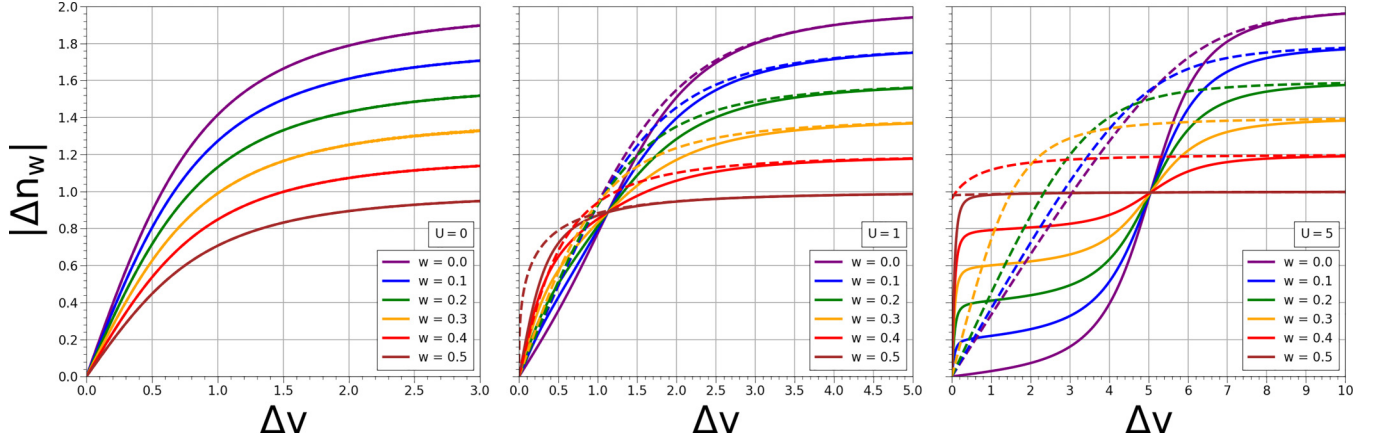
FIG. 18. Absolute value of the density of the Hubbard dimer bi-ensemble, plotted for various weight values as a function of Δv. Here we set $U = 0$ (left), $U = 1$ (center), and $U = 5$ (right). Dashed curves represent the ensemble HF approximation, and the solid curves are exact.

with coefficients determined to first order in U:

$$\alpha_0^{\mathrm{HF}} = 2t/c_0^{\mathrm{HF}} \qquad \alpha_1^{\mathrm{HF}} = -\Delta v_{\mathrm{eff},w}^2/2tc_1^{\mathrm{HF}}$$

$$\beta_0^{\pm \mathrm{HF}} = 1/2 \pm \Delta v_{\mathrm{eff},w}/c_0^{\mathrm{HF}} \qquad \beta_1^{\pm \mathrm{HF}} = \pm \Delta v_{\mathrm{eff},w}/c_1^{\mathrm{HF}}$$

$$c_0^{\mathrm{HF}} = 2\sqrt{4t^2 + \Delta v_{\mathrm{eff},w}^2} \qquad c_1^{\mathrm{HF}} = \Delta v_{\mathrm{eff},w}\sqrt{2 + \Delta v_{\mathrm{eff},w}^2/2t^2}.$$

Here the weight-dependent effective mean-field potential $\Delta v_{\mathrm{eff},w}$ takes the form [55]

$$\Delta v_{\mathrm{eff},w} = \Delta v + \frac{(1-3w)}{\overline{w}^2} \frac{U \Delta n_w^{\mathrm{HF}}}{2}, \qquad (55)$$

where Δn_w^{HF} is found from Eq. (32) with coefficients as above.

The self-consistent EHF density is found numerically throughout this work by solving Eq. (A2). Plots of the exact/EHF self-consistent site-occupation differences are included below in Fig. 18 for various interaction strengths, $U = 0$, 1, and 5. Here and for the remainder of this section, we denote the exact solution using solid curves and the EHF approximation using dashed curves. Looking at the left panel ($U = 0$) of Fig. 18, the EHF approximation agrees with the exact density, as expected in the limit of weak correlation. One can see that the exact/EHF densities (regardless of weight) begin to differ as U is increased, but must always match at the origin (where $\Delta v = \Delta n_w = 0$) and as $\Delta v \to \infty$ (where $|\Delta n_w| = 2\overline{w}$). This behavior would be expected to hold for larger U values, although as noted previously in Ref. [55], there exists a critical interaction strength U_{crit} at which nonphysical behavior is observed for symmetric dimers with bi-ensemble weight $w \geqslant 1/3$. This critical interaction strength is

$$U_{\mathrm{crit}} = \frac{\overline{w}}{3w - 1}. \qquad (56)$$

For $w \to \frac{1}{2}$, $U_{\mathrm{crit}} \to 1$. At this point, the energy expression for dimers with $U > U_{\mathrm{crit}}$ have multiple degenerate minima. This explains the deviation from expected behavior for $w = 0.4$, 0.5 in the right panel of Fig. 18, where both curves approach a finite value as $\Delta v \to 0$. We also plot the

exact/EHF bi-ensemble total energy below, using two interaction strengths ($U = 1$ and $U = 5$) to examine the EHF approximation in more detail. We depict this quantity as a function of Δv below in Fig. 19 and separate each w value in new plots to better illustrate the weight dependence of E_w and E_w^{HF}.

Analyzing Fig. 19, one can see that the EHF approximation obeys the variational principle for all viable weight values (where $w \leqslant 0.5$); as the weight of the first excited state is increased, both the exact/EHF energy becomes more positive for all Δv. We note that the EHF approximation always approaches the exact energy as $\Delta v \to \infty$, as shown previously for the ground state [52].

Below, we provide plots of the total weight-dependent correlation energy, as well as its kinetic/potential contributions,
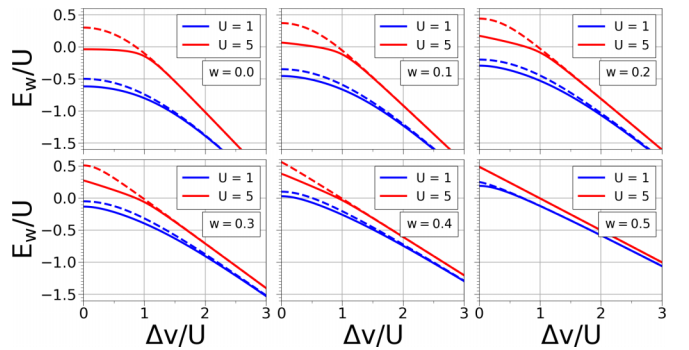
FIG. 19. Total energy of the Hubbard dimer bi-ensemble plotted as a function of $\Delta v/U$ for various w values. Dashed is HF and solid is exact.
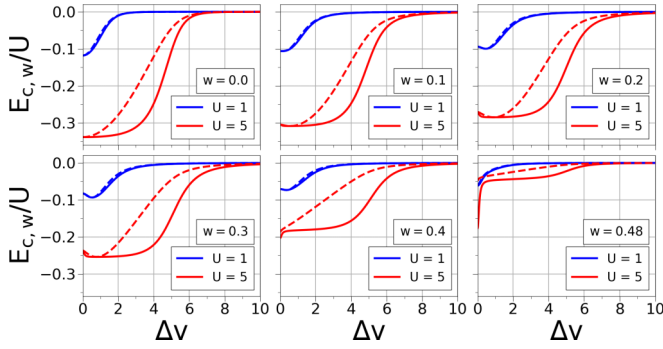
FIG. 20. Total correlation energy of the Hubbard dimer bi-ensemble plotted as a function of Δv for various w values. Dashed is HF and solid is exact.

in Figs. 20–22. Note that the definition of the EHF correlation energy is

$$E_{c,w}^{HF} = E_w[n_w] - E_w^{HF}[n_w^{HF}], \tag{57}$$

where each energy functional has been minimized by its respective weight-dependent self-consistent density.

Looking at Fig. 20, it is evident that the behavior of the correlation energy greatly depends upon the value of w. We find that the inequality relating the exact/approximate correlation energy holds for all ensembles (i.e., $E_c^{HF} \geqslant E_c$ for all weights). We show that a different trend exists for the kinetic/potential correlation components, as the inequalities describing the ground state ($T_c^{HF} \leqslant T_c$ and $U_c^{HF} \leqslant U_c$) no longer apply for ensembles with $w \neq 0$.

Note that for each of these quantities, the EHF approximate correlation energy matches the exact solution at $\Delta v = 0$, except for strongly correlated systems with $w \geqslant 1/3$ (due to the nonphysical behavior in this regime discussed previously).

It also is known that T_c^{HF} can become negative in the ground state of the Hubbard dimer [57], and we find this is also true when $w \neq 0$, but this is likely an artifact of lattice Hamiltonians that cannot occur in the real-space analog [50,54].
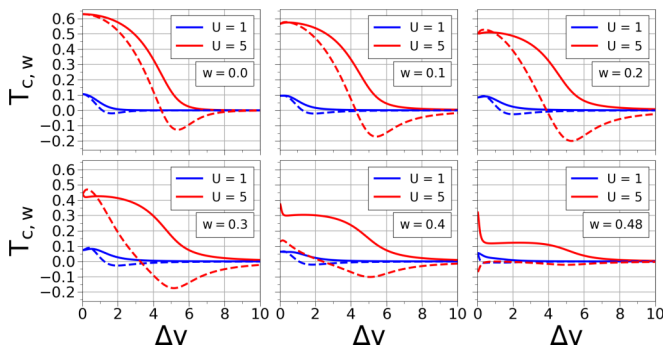
FIG. 21. Kinetic correlation energy of the Hubbard dimer bi-ensemble plotted as a function of Δv for various w values. Dashed is HF and solid is exact.
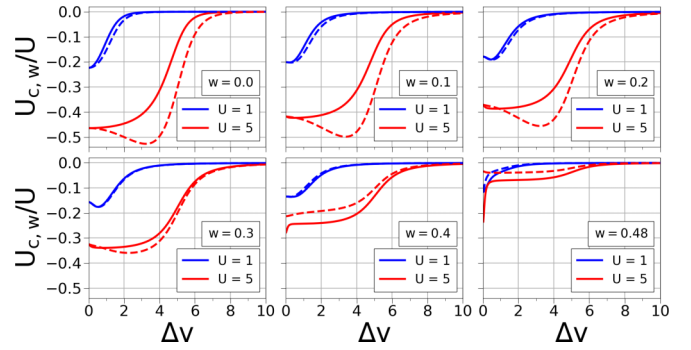
FIG. 22. Potential correlation energy of the Hubbard dimer bi-ensemble plotted as a function of Δv for various w values. Dashed is HF and solid is exact.

IV. CONCLUSIONS

The principal result of our work is the proving of several new conditions for use in ensemble DFT. The proofs follow exactly the same logical steps as in the ground-state case, as they are based on the variational principle and the nature of the kinetic and Coulomb repulsion operators. Because EDFT is based on a generalization of the variational principle, we were able to prove the same results using the minimizing density matrix instead of the ground-state wave function. That this is necessary can be seen from the fact that none of the proofs are valid for, e.g., an individual excited state.

Exact calculations in EDFT for realistic Hamiltonians are rare and challenging to perform. However, the two-site Hubbard model makes an ideal test case for novel results in DFT, as its tiny Hilbert space makes exact calculations almost trivial. It has the added benefit of covering both weak and strong correlation regimes. A crucial part of such tests is including asymmetric potentials so that the entire space of densities is examined.

Many of our exact conditions have been illustrated here on the Hubbard dimer. However, there are crucial differences between realistic Hamiltonians and lattice models. An example is the strictly correlated limit, where even the form of the leading corrections to strict correlation is different, as we show explicitly here. Hence, our results for the dimer do not contradict general results for realistic Hamiltonians. We also generalized earlier results for EDFT for the strongly correlated dimer, and our generalization is not restricted to being nearly symmetric.

We anticipate that, initially, our conditions will be built into new approximate functionals. Density functional approximations are more likely to produce accurate energies when they share the same constraints as the exact energy [38]. We note that our exact conditions apply to all allowed ensemble weights, suggesting they cannot be used to guide choices of weights. However, since these conditions are independent of weight, they are applicable to both Gross-Oliviera-Kohn schemes and any future schemes. These conditions also apply to the spin-restricted ensemble-referenced Kohn-Sham (REKS) [58,59] methods that have advanced EDFT-based methods forward.

One may also test a novel and existing EDFT approximation for its ability to reproduce these fundamental constraints

for any choice of weight. If the approximate functional fails an exact condition for certain weights, one would exclude those choices for use with that approximation. Another limitation of lattice models is that the approximations that are commonly used in realistic calculations cannot be applied. Thus they cannot be directly tested. But we can still illustrate the idea, as we have done for δ-PT2. This type of analysis can be used to guide next steps in developing approximate ensemble functionals.

APPENDIX: ANALYTIC SOLUTIONS OF THE HUBBARD DIMER BI-ENSEMBLE

Here, we report the analytic solutions of the Hubbard dimer that were used to create a bi-ensemble of the ground and first excited singlet states. Solving the dimer Hamiltonian [Eq. (28)], one obtains the energies:

$$E_i = \frac{2U}{3} + \frac{2r}{3} \cos\left[\theta + \frac{2\pi(i+1)}{3}\right], \qquad i = 0, 1. \quad \text{(A1)}$$

Here we have defined

$$r = \sqrt{3(4t^2 + \Delta v^2) + U^2},$$

$$\cos(3\theta) = \frac{9U(\Delta v^2 - 2t^2) - U^3}{r^3},$$

where t represents the hopping parameter, U the on-site electrostatic self-repulsion, and $\Delta v = v_2 - v_1$ the on-site potential difference. Furthermore, the wave function of each state may be written as

$$|\Psi_i\rangle = \alpha_i(|12\rangle + |21\rangle) + \beta_i^+ |11\rangle + \beta_i^- |22\rangle, \quad \text{(A2)}$$

with coefficients:

$$\alpha_i = \frac{2t(E_i - U)}{c_i E_i}, \quad \beta_i^\pm = \frac{U - E_i \pm \Delta v}{c_i},$$

$$c_i = \sqrt{2\left[\Delta v^2 + (E_i - U)^2\left(1 + 4t^2/E_i^2\right)\right]}.$$

Here, $|ij\rangle$ represents a state where an electron is present at sites i and j. These analytical expressions (both of the energy and wave function) may also be found in the Appendixes of Refs. [23] and [60]. We also make use of the derivation put forth by Deur *et al.* [23] to define:

$$T_{s,w} = -2t\sqrt{\overline{w}^2 - \Delta n_w^2/4} \qquad \text{(A3)}$$

$$E_{Hx,w} = \frac{U}{2}\left(1 + w - \frac{(3w - 1)}{\overline{w}^2}\frac{\Delta n_w^2}{4}\right). \qquad \text{(A4)}$$

[1] P. Hohenberg and W. Kohn, Inhomogeneous electron gas, Phys. Rev. **136**, B864 (1964).

[2] W. Kohn and L. J. Sham, Self-consistent equations including exchange and correlation effects, Phys. Rev. **140**, A1133 (1965).

[3] K. Burke, Perspective on density functional theory, J. Chem. Phys. **136**, 150901 (2012).

[4] A. D. Becke, Perspective: Fifty years of density-functional theory in chemical physics, J. Chem. Phys. **140**, 18A301 (2014).

[5] R. O. Jones, Density functional theory: Its origins, rise to prominence, and future, Rev. Mod. Phys. **87**, 897 (2015).

[6] P. Morgante and R. Peverati, The devil in the details: A tutorial review on some undervalued aspects of density functional theory calculations, Int. J. Quantum. Chem. **120**, e26332 (2020).

[7] C. A. Ullrich, *Time-dependent density-functional theory: concepts and applications* (Oxford University Press, Oxford, 2011).

[8] E. Runge and E. K. U. Gross, Density-functional theory for time-dependent systems, Phys. Rev. Lett. **52**, 997 (1984).

[9] M. Casida, Time-dependent density functional response theory of molecular systems: Theory, computational methods, and functionals, in *Recent Developments and Applications of Modern Density Functional Theory*, Vol. 4, edited by J. M. Seminario (Elsevier, Amsterdam, 1996).

[10] M. A. Marques, N. T. Maitra, F. M. Nogueira, E. K. Gross, and A. Rubio, *Fundamentals of Time-Dependent Density Functional Theory*, Vol. 837 (Springer, Berlin, 2012).

[11] N. T. Maitra, Perspective: Fundamental aspects of time-dependent density functional theory, J. Chem. Phys. **144**, 220901 (2016).

[12] D. J. Tozer, Relationship between long-range charge-transfer excitation energy error and integer discontinuity in Kohn–Sham theory, J. Chem. Phys. **119**, 12697 (2003).

[13] B. G. Levine, C. Ko, J. Quenneville, and T. J. MartÍnez, Conical intersections and double excitations in time-dependent density functional theory, Mol. Phys. **104**, 1039 (2006).

[14] M. Huix-Rotllant, A. Ipatov, A. Rubio, and M. E. Casida, Assessment of dressed time-dependent density-functional theory for the low-lying valence states of 28 organic chromophores, Chem. Phys. **391**, 120 (2011).

[15] A. K. Theophilou, The energy density functional formalism for excited states, J. Phys. C **12**, 5419 (1979).

[16] E. K. U. Gross, L. N. Oliveira, and W. Kohn, Rayleigh-Ritz variational principle for ensembles of fractionally occupied states, Phys. Rev. A **37**, 2805 (1988).

[17] E. K. U. Gross, L. N. Oliveira, and W. Kohn, Density-functional theory for ensembles of fractionally occupied states. I. Basic formalism, Phys. Rev. A **37**, 2809 (1988).

[18] Z.-h. Yang, J. R. Trail, A. Pribram-Jones, K. Burke, R. J. Needs, and C. A. Ullrich, Exact and approximate Kohn-Sham potentials in ensemble density-functional theory, Phys. Rev. A **90**, 042501 (2014).

[19] A. Pribram-Jones, Z.-H. Yang, J. R. Trail, K. Burke, R. J. Needs, and C. A. Ullrich, Excitations and benchmark ensemble density functional theory for two electrons, J. Chem. Phys. **140**, 18A541 (2014).

[20] Z.-h. Yang, A. Pribram-Jones, K. Burke, and C. A. Ullrich, Direct extraction of excitation energies from ensemble density-functional theory, Phys. Rev. Lett. **119**, 033003 (2017).

[21] T. Gould and S. Pittalis, Hartree and exchange in ensemble density functional theory: Avoiding the nonuniqueness disaster, Phys. Rev. Lett. **119**, 243001 (2017).

[22] K. Deur and E. Fromager, Ground and excited energy levels can be extracted exactly from a single ensemble density-functional theory calculation, J. Chem. Phys. **150**, 094106 (2019).

[23] K. Deur, L. Mazouin, and E. Fromager, Exact ensemble density functional theory for excited states in a model system: Investigating the weight dependence of the correlation energy, Phys. Rev. B **95**, 035120 (2017).

[24] T. Gould and S. Pittalis, Density-driven correlations in many-electron ensembles: Theory and application for excited states, Phys. Rev. Lett. **123**, 016401 (2019).

[25] E. Fromager, Individual correlations in ensemble density functional theory: State-and density-driven decompositions without additional Kohn-Sham systems, Phys. Rev. Lett. **124**, 243001 (2020).

[26] T. Gould and S. Pittalis, Density-driven correlations in ensemble density functional theory: Insights from simple excitations in atoms, Aust. J. Chem. **73**, 714 (2020).

[27] T. Gould, G. Stefanucci, and S. Pittalis, Ensemble density functional theory: Insight from the fluctuation-dissipation theorem, Phys. Rev. Lett. **125**, 233001 (2020).

[28] T. Gould and L. Kronik, Ensemble generalized Kohn–Sham theory: The good, the bad, and the ugly, J. Chem. Phys. **154**, 094125 (2021).

[29] T. Gould, Approximately self-consistent ensemble density functional theory: Toward inclusion of all correlations, J. Phys. Chem. Lett. **11**, 9907 (2020).

[30] P.-F. Loos and E. Fromager, A weight-dependent local correlation density-functional approximation for ensembles, J. Chem. Phys. **152**, 214101 (2020).

[31] C. Marut, B. Senjean, E. Fromager, and P.-F. Loos, Weight dependence of local exchange–correlation functionals in ensemble density-functional theory: Double excitations in two-electron systems, Faraday Discuss. **224**, 402 (2020).

[32] T. Gould, L. Kronik, and S. Pittalis, Double excitations in molecules from ensemble density functionals: Theory and approximations, Phys. Rev. A **104**, 022803 (2021).

[33] Z.-h. Yang, Second-order perturbative correlation energy functional in the ensemble density-functional theory, Phys. Rev. A **104**, 052806 (2021).

[34] F. Cernatic, B. Senjean, V. Robert, and E. Fromager, Ensemble density functional theory of neutral and charged excitations, Top. Curr. Chem. **380**, 4 (2022).

[35] F. Sagredo and K. Burke, Accurate double excitations from ensemble density functional calculations, J. Chem. Phys. **149**, 134103 (2018).

[36] J. P. Perdew, K. Burke, and M. Ernzerhof, Generalized gradient approximation made simple, Phys. Rev. Lett. **77**, 3865 (1996).

[37] M. Levy and J. P. Perdew, Hellmann-feynman, virial, and scaling requisites for the exact universal density functionals. shape of the correlation potential and diamagnetic susceptibility for atoms, Phys. Rev. A **32**, 2010 (1985).

[38] R. Pederson and K. Burke, The difference between molecules and materials: Reassessing the role of exact conditions in density functional theory, J. Chem. Phys. **159**, 214113 (2023).

[39] T. Gould, D. P. Kooi, P. Gori-Giorgi, and S. Pittalis, Electronic excited states in extreme limits via ensemble density functionals, Phys. Rev. Lett. **130**, 106401 (2023).

[40] Á. Nagy, Coordinate scaling and adiabatic connection formula for ensembles of fractionally occupied excited states, Int. J. Quantum Chem. **56**, 225 (1995).

[41] J. Hubbard, Electron correlations in narrow energy bands, Proc. R. Soc. London A **276**, 238 (1963).

[42] L. N. Oliveira, E. K. U. Gross, and W. Kohn, Density-functional theory for ensembles of fractionally occupied states. II. Application to the he atom, Phys. Rev. A **37**, 2821 (1988).

[43] Á. Nagy, Local virial theorem for ensembles of excited states, in *Concepts and Methods in Modern Theoretical Chemistry: Electronic Structure and Reactivity*, edited by S. K. Ghosh and P. C. Chattaraj (CRC Press, Boca Raton, 2013), p. 135.

[44] Á. Nagy, in *Recent Advances In Density Functional Methods: Part III* (World Scientific, Singapore, 2002), pp. 247–256.

[45] A. Nagy, Functional derivative of the kinetic energy functional for spherically symmetric systems, J. Chem. Phys. **135**, 044106 (2011).

[46] S. Pittalis, C. R. Proetto, A. Floris, A. Sanna, C. Bersier, K. Burke, and E. K. U. Gross, Exact conditions in finite-temperature density-functional theory, Phys. Rev. Lett. **107**, 163001 (2011).

[47] M. Levy and J. P. Perdew, Tight bound and convexity constraint on the exchange-correlation-energy functional in the low-density limit, and other formal tests of generalized-gradient approximations, Phys. Rev. B **48**, 11638 (1993).

[48] J. Harris, Adiabatic-connection approach to Kohn-Sham theory, Phys. Rev. A **29**, 1648 (1984).

[49] M. Ernzerhof, Construction of the adiabatic connection, Chem. Phys. Lett. **263**, 499 (1996).

[50] S. Crisostomo, M. Levy, and K. Burke, Can the Hartree–Fock kinetic energy exceed the exact kinetic energy? J. Chem. Phys. **157**, 154106 (2022).

[51] P.-O. Löwdin, Quantum theory of many-particle systems. III. Extension of the hartree-fock scheme to include degenerate systems and correlation effects, Phys. Rev. **97**, 1509 (1955).

[52] D. J. Carrascal, J. Ferrer, J. C. Smith, and K. Burke, The hubbard dimer: a density functional case study of a many-body problem, J. Phys.: Condens. Matter **27**, 393001 (2015).

[53] S. Giarrusso and A. Pribram-Jones, Møller-Plesset and density-fixed adiabatic connections for a model diatomic system at different correlation regimes, J. Chem. Theory Comput. **19**, 5835 (2023).

[54] S. Crisostomo, R. Pederson, J. Kozlowski, B. Kalita, A. C. Cancio, K. Datchev, A. Wasserman, S. Song, and K. Burke, Seven useful questions in density functional theory, Lett. Math Phys. **113**, 42 (2023).

[55] K. Deur, L. Mazouin, B. Senjean, and E. Fromager, Exploring weight-dependent density-functional approximations for ensembles in the Hubbard dimer, Eur. Phys. J. B **91**, 162 (2018).

[56] T. Gould, Z. Hashimi, L. Kronik, and S. G. Dale, Single excitation energies obtained from the ensemble "Homo–Lumo gap": Exact results and approximations, J. Phys. Chem. Lett. **13**, 2452 (2022).

[57] S. Giarrusso and A. Pribram-Jones, Comparing correlation components and approximations in Hartree–Fock and Kohn–Sham theories via an analytical test case study, J. Chem. Phys. **157**, 054102 (2022).

[58] M. Filatov and S. Shaik, Spin-restricted density functional approach to the open-shell problem, Chem. Phys. Lett. **288**, 689 (1998).

[59] M. Filatov and S. Shaik, A spin-restricted ensemble-referenced Kohn–Sham method and its application to diradicaloid situations, Chem. Phys. Lett. **304**, 429 (1999).

[60] J. C. Smith, A. Pribram-Jones, and K. Burke, Exact thermal density functional theory for a model system: Correlation components and accuracy of the zero-temperature exchange-correlation approximation, Phys. Rev. B **93**, 245131 (2016).